# Application of time-dependent density-functional theory to the dielectric function of various nonmetallic crystals

F. Kootstra, P. L. de Boeij, and J. G. Snijders
*Theoretical Chemistry, Materials Science Centre, Rijksuniversiteit Groningen, Nijenborgh 4, 9747 AG Groningen, The Netherlands*
(Received 14 December 1999; revised manuscript received 24 March 2000)

The dielectric function of a range of nonmetallic crystals of various lattice types is studied by means of a real-space and full-potential time-dependent density-functional method within the adiabatic local-density approximation. Results for the dielectric constant $\epsilon_\infty$ (at optical frequencies) are given for crystals in the sodium chloride, the fluoride, the wurtzite, the diamond, and the zinc-blende lattice structure. The frequency-dependent dielectric function $\epsilon(\omega)$ for the crystals in the diamond and zinc-blende lattice structure are also presented. We compare our calculated results with experimental data and other theoretical investigations. Our results for the dielectric constants $\epsilon_\infty$ and the dielectric functions $\epsilon(\omega)$ are in good agreement with the experimental values. The accuracy of the results is comparable to the one which is commonly found for time-dependent density-functional theory calculations on molecular systems. On average we find a deviation of 4–5 % from experiment for the group IV and III-V compounds in the wurtzite, zinc-blende and diamond lattice structure, 8–9 % for the II-VI and I-VII compounds in the zinc-blende and sodium chloride lattice structure, and up to 14% deviation for the fluoride lattice structure. The spectral features of the dielectric functions $\epsilon(\omega)$ appear in the calculations at somewhat too low energies compared to experiment.

## I. INTRODUCTION

After the introduction of the density-functional theory (DFT) (Refs. 1 and 2) in the 1960s, there have been numerous calculations on solids, predominantly in the local-density approximation (LDA). The accuracy of the results for many ground-state properties were very good, typically within a few percent of the experimental values. Therefore DFT has now become one of the standard methods in the field. Notable exceptions, however, are the dielectric constants of crystals, which are generally believed to be overestimated substantially by DFT-LDA. This failure is remarkable and in clear contrast with the success of DFT calculations on molecular systems[3–5] for which polarizabilities of molecules can be obtained typically to within 5% of the experimental values. The reason for the overestimation of the dielectric constants by DFT-LDA is often attributed to the underestimation of the band gap by LDA. There have been several attempts, within DFT, to go beyond LDA,[6–9] but all with limited success as far as the dielectric function is concerned. In the 1980s Runge and Gross[10] gave a sound basis for the time-dependent version of DFT (TDDFT). Nowadays TDDFT has been used successfully in atomic and molecular systems[11] and a lot of experience has been built up in this area. Most of the present DFT implementations for solids use pseudopotentials in combination with a plane-wave basis.[12–14] In this paper we present the results of our real-space approach[15] to TDDFT, which is a full-potential linear combination of atomic orbitals (LCAO) implementation. The calculated dielectric response functions for several crystals of various lattice types are compared with other theoretical investigations,[7,12,13,16–32] and with experimental data.[22,35–58] The different crystals, which we have studied, have the sodium chloride structure ($MX$ with $M=$Li, Na, K, Rb, Cs; $X=$F, Cl, Br, I, and $NY$ with $N=$Mg, Ca, Sr, Ba; $Y=$O, S, Se, Te) the fluoride structure ($MF_2$ with $M=$Ca, Sr, Cd, Ba), the wurtzite structure (BeO, BN, SiC, AlN, GaN, InN, ZnO, ZnS, CdS, CdSe), the diamond structure (C, Si, Ge), or the zinc-blende structure ($MX$ with $M=$Al, Ga, In; $X=P$, As, Sb, and $NY$ with $N=$Zn, Cd; $Y=$S, Se, Te). The outline of this paper is as follows. First we give a brief review of our (TD)DFT method and implementation.[15,59,60] Then, in the next section, we present our results for the dielectric constants and functions, and compare them with other theoretical calculations and (available) experimental data. Finally, in the last section, we draw the conclusions.

## II. METHOD

Our real-space approach to time-dependent density-functional theory for crystals, is based on the Amsterdam density functional band-structure (ADF-BAND) (Refs. 59 and 60) implementation for ground-state DFT. The Kohn-Sham equation[1,2] reads

$$H\psi_{n\mathbf{k}}(\mathbf{r})=[T+V_{\mathrm{C}}(\mathbf{r})+V_{\mathrm{XC}}(\mathbf{r})]\psi_{n\mathbf{k}}(\mathbf{r})=\epsilon_{n\mathbf{k}}\psi_{n\mathbf{k}}(\mathbf{r}), \quad (1)$$

in which $T$ is the kinetic energy operator, $V_{\mathrm{C}}$ the Coulomb potential due to the nuclear charges and the self-consistent electron density and $V_{\mathrm{XC}}$ is the exchange-correlation potential for which we used the LDA approximation in the Vosko-Wilk-Nusair parametrization.[61] The one-electron states $\psi_{n\mathbf{k}}(\mathbf{r})$ are expressed on a basis of Bloch functions $\varphi_{i\alpha\mathbf{k}}(\mathbf{r})$. At a particular $\mathbf{k}$ point in the Brillouin zone (BZ) the basis functions $\varphi_{i\alpha\mathbf{k}}(\mathbf{r})$ are obtained by constructing the Bloch combinations of the atomic one-centered functions $\chi_i$ according to

$$\varphi_{i\alpha\mathbf{k}}(\mathbf{r})=\sum_{\mathbf{R}} e^{i\mathbf{k}\cdot\mathbf{R}}\chi_i(\mathbf{r}-\mathbf{R}-\mathbf{s}_\alpha). \quad (2)$$

Here $\chi_i$ can be a numerical atomic orbital (NAO) or a Slater-type exponential function (STO) which are centered on atom

 

$\alpha$ at position $\mathbf{s}_\alpha$ in the crystal unit cell. The summation runs over all lattice points $\mathbf{R}$. The NAO's are obtained from the fully numerical Herman-Skillman (HS) program,[62] which solves the density-functional equations for the spherically symmetric atoms. This basis of NAO's is extended by STO's to a $3Z2P$ basis (triple zeta basis, augmented with two polarization functions). It is possible to use the frozen core approximation for the innermost atomic states. All matrix elements that involve these functions are evaluated using an accurate numerical integration scheme[59,63] which uses Gauss quadrature formulas. The Coulomb potentials $V_\alpha$ which are due to the spherically symmetric atomic densities $\rho_\alpha$ are provided by the HS program. The crystal Coulomb potential is then given by

$$\mathrm{V_C}(\mathbf{r}) = \sum_\alpha \mathrm{V}_\alpha(\mathbf{r}) + \int \frac{\rho_{\mathrm{def}}(\mathbf{r}')}{|\mathbf{r}-\mathbf{r}'|}\, d\mathbf{r}', \tag{3}$$

in which the deformation density $\rho_{\mathrm{def}}$ is defined as the difference between the crystal charge distribution and the superposition of atomic densities. The deformation density is obtained by summing over products of basis functions, which makes the direct evaluation of the second term in Eq. (3) laborious. The problem is solved by the use of a fitting procedure[64], in which the density is expanded on a basis of fit functions

$$\rho_{\mathrm{def}}(\mathbf{r}) \approx \sum_i c_i f_i(\mathbf{r}). \tag{4}$$

Here the fitfunctions $f_i$ are the totally symmetric Bloch combinations of the atomic Slater-type exponential functions $r^{n-1}e^{-\alpha r}Z_{lm}(\Omega)$, where $Z_{lm}(\Omega)$ are the real-valued spherical harmonics. The corresponding Coulomb potentials $f_i^{\mathrm{C}}$ of these fit functions can easily be evaluated analytically:

$$f_i^{\mathrm{C}}(\mathbf{r}) = \int \frac{f_i(\mathbf{r}')}{|\mathbf{r}-\mathbf{r}'|} d\mathbf{r}'. \tag{5}$$

The Coulomb integrals can now be constructed according to

$$V_{\mathrm{C}}(\mathbf{r}) \approx \sum_\alpha V_\alpha(\mathbf{r}) + \sum_i c_i f_i^{\mathrm{C}}(\mathbf{r}). \tag{6}$$

The fit coefficients $c_i$ are determined by a least-squares solution of Eq. (4), where the total amount of deformation charge is constrained to vanish. The integrals over the BZ are evaluated by using a quadratic tetrahedron method.[65,66]

In the time-dependent extension[15] we employ a lattice periodic (microscopic) effective scalar potential $v_{eff}(\mathbf{r},t)$, in combination with a uniform (macroscopic) electric field $\mathbf{E}_{mac}(\mathbf{r},t)$. This macroscopic electric field can be represented by a uniform vector potential $\mathbf{A}(\mathbf{r},t)$. In this scheme the time-dependent Kohn-Sham equation reads

$$i\frac{\partial}{\partial t}\psi_n(\mathbf{r},t) = \left(\frac{1}{2}\left|-i\nabla + \frac{1}{c}\mathbf{A}_{eff}(\mathbf{r},t)\right|^2 + v_{eff}(\mathbf{r},t)\right)\psi_n(\mathbf{r},t), \tag{7}$$

so the particles move in time-dependent effective potentials $\{v_{eff}(\mathbf{r},t), \mathbf{A}_{eff}(\mathbf{r},t)\}$ which comprise the externally applied potentials, and the Coulomb and exchange-correlation contributions of the perturbed density and current distributions. For the exchange-correlation contribution to the scalar potential we used the adiabatic local-density approximation (ALDA). We neglected such a contribution to the vector potential. The TDDFT equations are solved in an iterative scheme, in which the macroscopic electric field is kept fixed and the microscopic potential is updated in each cycle, until self-consistency is established. The first-order density change $\delta\rho(\mathbf{r},\omega)$ (Fourier transformed) is obtained from the first-order potential change $\delta v_{eff}(\mathbf{r}',\omega)$ according to

$$\delta\rho(\mathbf{r},\omega) = \int \left[\frac{i}{\omega}\chi_{\rho\mathbf{j}}(\mathbf{r},\mathbf{r}',\omega)\cdot\mathbf{E}_{mac}(\omega) + \chi_{\rho\rho}(\mathbf{r},\mathbf{r}',\omega)\,\delta v_{eff}(\mathbf{r}',\omega)\right] d\mathbf{r}', \tag{8}$$

where the various response kernels $\chi_{ab}(\mathbf{r},\mathbf{r}',\omega)$ can be obtained from the following expression:

$$\chi_{ab}(\mathbf{r},\mathbf{r}',\omega) = \frac{1}{V_{BZ}}\sum_{n,n'}\int_{V_{BZ}} (f_{n\mathbf{k}} - f_{n'\mathbf{k}}) \times \frac{[\psi^*_{n\mathbf{k}}(\mathbf{r})\hat{a}\,\psi_{n'\mathbf{k}}(\mathbf{r})][\psi^*_{n'\mathbf{k}}(\mathbf{r}')\hat{b}\,\psi_{n\mathbf{k}}(\mathbf{r}')]}{\epsilon_{n\mathbf{k}} - \epsilon_{n'\mathbf{k}} + \omega + i\eta} d\mathbf{k}, \tag{9}$$

by substituting either $\hat{\rho} = 1$ or $\hat{\mathbf{j}} = -i(\vec{\nabla} - \overleftarrow{\nabla})/2$ (the arrows indicate whether the left or right side should be differentiated) for the operators $\hat{a}$ and $\hat{b}$. Here $f_{n\mathbf{k}}$ is the occupation number and $\epsilon_{n\mathbf{k}}$ the energy eigenvalue of the Bloch orbital $\psi_{n\mathbf{k}}$ of the ground state. They are labeled by the band index $n$ and wave vector $\mathbf{k}$. The integrations over the Bloch vector $\mathbf{k}$ in Eq. (9) can be restricted to the irreducible part of the Brillouin zone (IBZ) due to the transformation properties of the Bloch functions, and they are evaluated numerically using the following quadrature (see Appendix B of Ref. 15):

$$\frac{1}{V_{IBZ}}\int_{IBZ} \frac{(f_{n\mathbf{k}} - f_{n'\mathbf{k}})}{\epsilon_{n\mathbf{k}} - \epsilon_{n'\mathbf{k}} + \omega + i\eta} g(\mathbf{k})\, d\mathbf{k} = \sum_{\mathbf{k}_j} w_{nn'\mathbf{k}_j}(\omega) g(\mathbf{k}_j). \tag{10}$$

The singular behavior of the denominator can thus be handled analytically, and is incorporated in the $\omega$-dependent integration weights $w_{nn'\mathbf{k}_j}(\omega)$. Using a fitting procedure similar to the one used in the ground-state calculation, we can obtain the potential change $\delta v_{eff}$ as a function of the density change $\delta\rho$. The induced macroscopic polarization $\mathbf{P}_{mac}$ is defined as the time integral of the average induced current density $\delta\mathbf{j}$,

$$\mathbf{P}_{mac}(\mathbf{r},t) = -\frac{1}{V}\int^t \int_V \delta\mathbf{j}(\mathbf{r}',t')\, d\mathbf{r}'\, dt'. \tag{11}$$

The Cartesian components of the electric susceptibility can then be obtained, as soon as self-consistency in the density change $\delta\rho$ is achieved. From $\mathbf{P}_{mac}(\omega) = \chi_e(\omega)\cdot\mathbf{E}_{mac}(\omega)$ it follows that

TABLE I. Optical dielectric constants for crystals in the sodium chloride lattice structure.

| Solid | $a$ (Å) (Ref. 16) | This work | Experiment | Error (%) | Other theory | Method [a b c d] |
|---|---|---|---|---|---|---|
| LiF | 4.017 | 2.01 | 1.92 (Ref. 35) | 5 | 3.60 (Ref. 16) | UR,FP,OLCAO,QP |
| | | | 1.96 (Ref. 56) | 3 | 4.09 (Ref. 16) | UR,FP,OLCAO |
| LiCl | 5.129 | 2.97 | 2.68 (Ref. 35) | 11 | 3.07 (Ref. 7) | DM,PP,PW,LF,XC |
| | | | | | 2.17 (Ref. 16) | UR,FP,OLCAO,QP |
| | | | | | 3.50 (Ref. 16) | UR,FP,OLCAO |
| LiBr | 5.507 | 3.42 | 3.00 (Ref. 35) | 14 | 3.03 (Ref. 16) | UR,FP,OLCAO,QP |
| | | | | | 5.64 (Ref. 16) | UR,FP,OLCAO |
| LiI | 6.000 | 3.90 | 3.40 (Ref. 35) | 15 | 2.30 (Ref. 16) | UR,FP,OLCAO,QP |
| | | | | | 3.61 (Ref. 16) | UR,FP,OLCAO |
| NaF | 4.620 | 1.87 | 1.74 (Ref. 35) | 7 | 1.74 (Ref. 16) | UR,FP,OLCAO,QP |
| | | | | | 2.66 (Ref. 16) | UR,FP,OLCAO |
| | | | | | 1.670 (Ref. 17) | TDPT,EP,LAPW |
| | | | | | 1.317 (Ref. 17) | TDPT,EP,LAPW,QP |
| NaCl | 5.630 | 2.66 | 2.33 (Ref. 35) | 14 | 1.88 (Ref. 16) | UR,FP,OLCAO,QP |
| | | | | | 3.48 (Ref. 16) | UR,FP,OLCAO |
| | | | | | 2.529 (Ref. 17) | TDPT,EP,LAPW |
| | | | | | 1.819 (Ref. 17) | TDPT,EP,LAPW,QP |
| NaBr | 5.937 | 2.58 | 2.60 (Ref. 35) | 1 | 1.91 (Ref. 16) | UR,FP,OLCAO,QP |
| | | | | | 3.05 (Ref. 16) | UR,FP,OLCAO |
| | | | | | 2.762 (Ref. 17) | TDPT,EP,LAPW |
| | | | | | 2.194 (Ref. 17) | TDPT,EP,LAPW,QP |
| NaI | 6.473 | 3.39 | 2.98 (Ref. 35) | 14 | 2.49 (Ref. 16) | UR,FP,OLCAO,QP |
| | | | | | 2.76 (Ref. 16) | UR,FP,OLCAO |
| | | | | | 3.394 (Ref. 17) | TDPT,EP,LAPW |
| | | | | | 2.353 (Ref. 17) | TDPT,EP,LAPW,QP |
| KF | 5.347 | 1.82 | 1.84 (Ref. 35) | 1 | 1.39 (Ref. 16) | UR,FP,OLCAO,QP |
| | | | | | 2.15 (Ref. 16) | UR,FP,OLCAO |
| | | | | | 1.588 (Ref. 17) | TDPT,EP,LAPW |
| | | | | | 1.230 (Ref. 17) | TDPT,EP,LAPW,QP |
| KCl | 6.290 | 2.31 | 2.17 (Ref. 35) | 6 | 2.43 (Ref. 16) | UR,FP,OLCAO,QP |
| | | | | | 2.87 (Ref. 16) | UR,FP,OLCAO |
| | | | | | 2.268 (Ref. 17) | TDPT,EP,LAPW |
| | | | | | 1.493 (Ref. 17) | TDPT,EP,LAPW,QP |
| KBr | 6.600 | 2.51 | 2.35 (Ref. 35) | 7 | 2.17 (Ref. 16) | UR,FP,OLCAO,QP |
| | | | | | 2.62 (Ref. 16) | UR,FP,OLCAO |
| | | | | | 2.680 (Ref. 17) | TDPT,EP,LAPW |
| | | | | | 1.779 (Ref. 17) | TDPT,EP,LAPW,QP |
| KI | 7.066 | 3.08 | 2.63 (Ref. 35) | 17 | 2.18 (Ref. 16) | UR,FP,OLCAO,QP |
| | | | | | 2.81 (Ref. 16) | UR,FP,OLCAO |
| | | | | | 2.842 (Ref. 17) | TDPT,EP,LAPW |
| | | | | | 1.867 (Ref. 17) | TDPT,EP,LAPW,QP |
| RbF | 5.640 | 1.87 | 1.93 (Ref. 35) | 3 | 1.10 (Ref. 16) | UR,FP,OLCAO,QP |
| | | | | | 1.14 (Ref. 16) | UR,FP,OLCAO |
| RbCl | 6.581 | 2.28 | 2.17 (Ref. 35) | 5 | 1.38 (Ref. 16) | UR,FP,OLCAO,QP |
| | | | | | 1.43 (Ref. 16) | UR,FP,OLCAO |
| RbBr | 6.854 | 2.43 | 2.34 (Ref. 35) | 4 | 1.77 (Ref. 16) | UR,FP,OLCAO,QP |
| | | | | | 2.00 (Ref. 16) | UR,FP,OLCAO |
| RbI | 7.342 | 2.65 | 2.59 (Ref. 35) | 2 | 1.37 (Ref. 16) | UR,FP,OLCAO,QP |
| | | | | | 1.50 (Ref. 16) | UR,FP,OLCAO |
| CsF | 6.010 | 1.84 | | | | |
| CsCl | 7.140 | 2.04 | 2.30 (Ref. 35) | 11 | | |
| CsBr | 7.420 | 2.21 | 2.43 (Ref. 35) | 9 | | |
| CsI | 7.900 | 2.40 | 2.63 (Ref. 35) | 9 | | |

TABLE I. (*Continued*).

| Solid | $a$ (Å) (Ref. 16) | This work | Experiment | Error (%) | Other theory | Method [a b c d] |
|---|---|---|---|---|---|---|
| MgO | 4.210 | 3.20 | 2.95 (Ref. 35) | 8 | 3.10 (Ref. 16) | UR,FP,OLCAO,QP |
| | | | | | 4.28 (Ref. 16) | UR,FP,OLCAO |
| MgS | 5.203 | 5.37 | 4.84 (Ref. 35) | 11 | 4.52 (Ref. 16) | UR,FP,OLCAO,QP |
| | | | | | 5.12 (Ref. 16) | UR,FP,OLCAO |
| MgSe | 5.460 | 6.25 | 5.28 (Ref. 35) | 18 | | |
| CaO | 4.810 | 2.90 | 3.27 (Ref. 35) | 11 | 1.66 (Ref. 16) | UR,FP,OLCAO,QP |
| | | | | | 3.22 (Ref. 16) | UR,FP,OLCAO |
| CaS | 5.690 | 4.30 | 4.24 (Ref. 35) | 1 | 3.01 (Ref. 16) | UR,FP,OLCAO,QP |
| | | | | | 4.47 (Ref. 16) | UR,FP,OLCAO |
| CaSe | 5.920 | 4.81 | 4.58 (Ref. 35) | 5 | | |
| SrO | 5.160 | 3.26 | 3.35 (Ref. 35) | 3 | 1.90 (Ref. 16) | UR,FP,OLCAO,QP |
| | | | | | 3.04 (Ref. 16) | UR,FP,OLCAO |
| SrS | 6.020 | 4.37 | 4.09 (Ref. 35) | 7 | 2.78 (Ref. 16) | UR,FP,OLCAO,QP |
| | | | | | 3.68 (Ref. 16) | UR,FP,OLCAO |
| SrSe | 6.240 | 4.77 | 4.33 (Ref. 35) | 10 | | |
| SrTe | 6.480 | 5.88 | 4.91 (Ref. 35) | 19 | | |
| BaO | 5.520 | 3.36 | 3.68 (Ref. 35) | 9 | 2.90 (Ref. 16) | UR,FP,OLCAO,QP |
| | | | | | 4.01 (Ref. 16) | UR,FP,OLCAO |
| BaS | 6.380 | 4.07 | 4.26 (Ref. 35) | 4 | | |
| BaSe | 6.600 | 4.50 | 4.48 (Ref. 35) | 1 | | |
| BaTe | 6.980 | 4.94 | 4.71 (Ref. 35) | 5 | | |

[a]TDPT: time-dependent perturbation theory; DM: dielectric matrix; UR: uncoupled response.
[b]FP: full potential; PP: pseudopotential; EP: empirical potential.
[c]PW: plane wave; LAPW: linearized augmented plane wave; OLCAO: orthogonalized linear combination of atomic orbitals.
[d]XC: exchange-correlation effects; QP: quasiparticle energy shift; LF: local field effects.

$$[\chi_e(\omega)]_{ij}=\left\{-\frac{1}{V\omega^2}\int_V[\delta\mathbf{j}_p(\mathbf{r},\omega)-\delta\mathbf{j}_p(\mathbf{r},0)]_i\,d\mathbf{r}\right\}\Bigg|_{\mathbf{E}_{mac}(\omega)=-i\omega\mathbf{e}_j}, \qquad (12)$$

in which the macroscopic field $\mathbf{E}_{mac}(\omega)$ is directed along the unit vector $\mathbf{e}_j$ and the induced paramagnetic current $\delta\mathbf{j}_p(\mathbf{r},\omega)$ is given by

$$\delta\mathbf{j}_p(\mathbf{r},\omega)=\int\left(\frac{i}{\omega}\chi_{\mathbf{jj}}(\mathbf{r},\mathbf{r}',\omega)\cdot\mathbf{E}_{mac}(\omega)+\chi_{\mathbf{j}\rho}(\mathbf{r},\mathbf{r}',\omega)\,\delta v_{eff}(\mathbf{r}',\omega)\right)d\mathbf{r}'. \qquad (13)$$

## III. DIELECTRIC CONSTANTS

The dielectric constants were calculated for a wide variety of nonmetallic crystals to test the accuracy of our implementation[15] and to benchmark the performance of our calculation method. The crystals for which we calculated the dielectric constants $\epsilon_\infty$ can be ordered into five groups according to their lattice structures. They have either the sodium chloride, the fluoride, the wurtzite, the diamond, or the zinc-blende lattice structure. For all lattice structures we compared our result for $\epsilon_\infty$ with those found by a wide variety of other theoretical approaches.[7,12,13,16–32] This comparison is made to demonstrate the accuracy of our method, and to show the importance of the inclusion of both Coulomb and exchange-correlation contributions in response calculations. We can classify the other approaches according to the way they treat these contributions. If one calculates the $\chi_0$ response directly from the ground-state solutions, without inclusion of any Coulomb or exchange-correlation contributions in the response part, we classify them as uncoupled response (UR). Other approaches include the Coulomb interaction (and possibly also exchange-correlation contributions), but involve the inversion of a large dielectric matrix (DM). Usually these methods use plane waves in combination with pseudopotentials, and they include the macroscopic contributions to the field in the Coulomb term, for which they need a special treatment of the long wavelenght limit. The density-functional perturbation theory (DFPT) (Ref. 23) closely resembles our method[15] in the way the response calculation is performed. DFPT only treats static perturbations, whereas we consider time-dependent perturbations. Where we use a LCAO basis in a full-potential method, the DFPT implementation uses pseudopotentials and plane waves. Furthermore, DFPT uses a plane-wave expansion of the density to solve the Poisson equation and to separate microscopic and macroscopic contributions, where we use an expansion in Slater-type fit functions, which treat the cusps correctly, in combination with a screening technique. In the present work the time-dependent polarization is directly related to the current density through Eq. (11), which is consistent with the use of the polarization current $d\mathbf{P}/dt$ in the macroscopic Maxwell equations. It is exactly this polarization that is measured in experiment. The static susceptibility can be obtained

TABLE II. Optical dielectric constants for crystals in the fluoride lattice structure.

| Solid | $a$ (Å) (Ref. 16) | This work | Experiment | Error (%) | Other theory | Method [a b c d] |
|---|---|---|---|---|---|---|
| $CaF_2$ | 5.460 | 1.78 | 2.04 (Ref. 35) | 13 | 1.49 (Ref. 16) | UR,FP,OLCAO,QP |
| | | | 1.50 (Ref. 47) | 19 | 2.02 (Ref. 16) | UR,FP,OLCAO |
| | | | 1.50 (Ref. 48) | 19 | 2.02 (Ref. 32) | UR,FP,OLCAO |
| | | | | | 1.80 (Ref. 32) | UR,FP,OLCAO,SIC |
| | | | | | 1.49 (Ref. 32) | UR,FP,OLCAO,QP |
| $SrF_2$ | 5.800 | 1.89 | 2.06 (Ref. 35) | 8 | 1.12 (Ref. 16) | UR,FP,OLCAO,QP |
| | | | | | 1.23 (Ref. 16) | UR,FP,OLCAO |
| $CdF_2$ | 5.388 | 2.48 | 3.14 (Ref. 35) | 21 | 6.90 (Ref. 16) | UR,FP,OLCAO,QP |
| | | | | | 8.00 (Ref. 16) | UR,FP,OLCAO |
| $BaF_2$ | 6.200 | 1.97 | 2.15 (Ref. 35) | 8 | 1.07 (Ref. 16) | UR,FP,OLCAO,QP |
| | | | | | 1.12 (Ref. 16) | UR,FP,OLCAO |

[a]UR: uncoupled response.
[b]FP: full potential.
[c]OLCAO: orthogonalized linear combination of atomic orbitals.
[d]QP: quasiparticle energy shift; SIC: self-interaction correction.

in a gauge invariant way from the paramagnetic current [Eq. (12)]. This way we establish a proper behavior for the static limit ($\omega \to 0$). Note that in this limit the resulting expressions become identical to those used in the static DFPT method. However, we do not need to transform dipole matrix elements into the velocity form.

### A. Sodium chloride structure

The sodium chloride lattice structure calculations were done by using a $3Z2P$ NAO/STO basis (basis $V$ in the BAND program), which consists of a triple zeta basis augmented with two polarization functions. For integration in the reciprocal space, it turned out to be sufficient for these materials to use 15 symmetry unique **k** points in the IBZ. We found that the Kohn-Sham energy gap in the LDA approximation underestimates the optical-absorption energies by about 40%, as is well known.[16,17] In Table I we list the lattice constants for the investigated crystals, our results for the dielectric constant ($\epsilon_\infty$) together with the experimental values,[35] and the relative errors. We have also included the theoretical results of Ching *et al.*,[16] who use full-potential (FP) wave functions but UR, and of Li *et al.*,[17] who use an empirical potential (EP) in a linearized augmented-plane-wave (LAPW) method. The results for $\epsilon_\infty$ in our work are obtained without shifting the virtual energy bands, which is known as the scissors operator $\Delta$ or quasiparticle (QP) energy shift. It can be seen that our results for $\epsilon_\infty$ show an average deviation from experiment of about 8%. The results of Ching *et al.*[16] (UR, FP) were considerably less accurate. Their use of a QP shift does not systematically improve their results for $\epsilon_\infty$, as can be seen in Table I. Other calculations by Li *et al.*[17] (LAPW, EP) found for the alkali halides $MX$ ($M$=Na, K; $X$=F, Cl, Br, I) results for $\epsilon_\infty$ which deviate, without the use of a QP shift, up to 15% from experiment. A QP shift made their results even worse, up to 33% deviation from experiment. Without using a QP shift, we get $\epsilon_\infty$ values for these alkali halides which are more accurate compared to those found by the other methods.[16,17]

### B. Fluoride structure

Using the same $3Z2P$ NAO/STO basis and **k** space integration accuracy as for the sodium chloride structures, we calculated the dielectric constants $\epsilon_\infty$ of four fluoride crystals ($CaF_2$, $SrF_2$, $CdF_2$, and $BaF_2$). In these compounds LDA underestimates the Kohn-Sham energy gap, compared to the optical-absorption energy, around 30%. Our results for the dielectric constants are listed in Table II together with the experimental values of Refs. 35, 47, and 48, and relative errors compared to these experimental values. We have also included other theoretical results.[16,32] The results for the dielectric constants found by Ching *et al.*[16] (UR, FP) deviate, without the use of a QP shift, up to 47% from experimental data of Lines.[35] When using a QP shift this deviation increased up to 55% (for $CdF_2$ even more than 100%). The experimental value for $CaF_2$ shows a large variation, from 2.04 found by Lines[35] to 1.50 found by Barth *et al.*[47] and Stephan *et al.*[48] The calculated $\epsilon_\infty$ value for $CaF_2$ by Gan *et al.*,[32] who uses a FP method, varies from 2.02 (UR) (which agrees with the experiment by Lines[35]) to 1.80, when allowing for self interacting corrections (SIC), and to 1.49, when using a QP shift (which agrees with the experiment by Barth *et al.*[47] and Stephan *et al.*[48]). Our results for the dielectric constants $\epsilon_\infty$, obtained without the use of a QP shift, show an average deviation of about 14% from experiment, and they are the best values up to date, but we do not achieve the same accuracy as for the other lattice structures. In the case of $CaF_2$ our result for $\epsilon_\infty$ is in between the two experimetal ones.[35,47]

### C. Wurtzite structure

As an example of anisotropic crystals, we studied several crystals of the wurtzite structure. For these calculations the same $3Z2P$ NAO/STO basis and **k** space integration accuracy was used as for the sodium chloride structures. The wurtzite structure is very similar to the zinc-blende structure (see later) and only differs in the stacking of the layers along the [111] direction. Therefore many crystals like SiC, ZnS, CdS, etc. exist in both forms. Ideally the $c/a$ ratio equals

TABLE III. Optical dielectric constant and anisotropy for crystals in the wurtzite lattice structure.

| Crystal | Lattice Parameters (Ref. 18) (Å) | | | This work | | Experiment | Error | Other theory | | Method |
|---|---|---|---|---|---|---|---|---|---|---|
| | $a$ | $c$ | $u$ | $\bar{\epsilon}_\infty$ [a] | $\Delta\epsilon_\infty$ [b] | $\bar{\epsilon}_\infty$ | % | $\bar{\epsilon}_\infty$ | $\Delta\epsilon_\infty$ | [c d e f] |
| BeO | 2.698 | 4.380 | 0.378 | 2.92 | 0.05 | | | 2.76 | 0.02 (Ref. 18) | UR,FP,LCAO |
| BN | 2.536 | 4.199 | 0.375 | 4.17 | 0.38 | | | 4.07 | 0.25 (Ref. 18) | UR,FP,LCAO |
| | | | | | | | | 4.57 | 0.18 (Ref. 19) | UR,PP,PW,LF |
| | | | | | | | | 4.14 | 0.13 (Ref. 20) | UR,ASA,LMTO |
| SiC | 3.076 | 5.048 | 0.375 | 6.93 | 0.75 | | | 8.09 | 1.17 (Ref. 18) | UR,FP,LCAO |
| AlN | 3.110 | 4.980 | 0.382 | 4.56 | −0.01 | 4.84 (Ref. 51) | 6 | 4.27 | 1.19 (Ref. 18) | UR,FP,LCAO |
| | | | | | | 4.68 (Ref. 52) | 3 | 4.51 | 0.28 (Ref. 19) | UR,PP,PW,LF |
| | | | | | | | | 3.86 | 0.14 (Ref. 20) | UR,ASA,LMTO |
| GaN | 3.190 | 5.189 | 0.375 | 5.31 | 0.30 | 5.2 (Ref. 53) | 2 | 9.53 | 2.44 (Ref. 18) | UR,FP,LCAO |
| | | | | | | 5.7 (Ref. 54) | 7 | 5.56 | 0.06 (Ref. 19) | UR,PP,PW,LF |
| | | | | | | | | 4.68 | 0.09 (Ref. 20) | UR,ASA,LMTO |
| | | | | | | | | 5.47 | 0.22 (Ref. 21) | UR,PP |
| InN | 3.533 | 5.692 | 0.375 | 8.78 | −1.13 | 8.4 (Ref. 55) | 5 | 7.39 | 1.01 (Ref. 18) | UR,FP,LCAO |
| | | | | | | | | 7.16 | 0.33 (Ref. 20) | UR,ASA,LMTO |
| ZnO | 3.249 | 5.207 | 0.375 | 4.26 | −0.03 | | | 8.62 | 0.86 (Ref. 18) | UR,FP,LCAO |
| ZnS | 3.811 | 6.234 | 0.375 | 5.71 | 0.30 | | | 6.81 | 1.58 (Ref. 18) | UR,FP,LCAO |
| CdS | 4.137 | 6.714 | 0.375 | 5.22 | 0.30 | | | 5.07 | −0.03 (Ref. 18) | UR,FP,LCAO |
| CdSe | 4.299 | 7.015 | 0.375 | 6.11 | 0.21 | | | 4.94 | −0.03 (Ref. 18) | UR,FP,LCAO |

[a] $\bar{\epsilon}_\infty = \frac{1}{3}(\epsilon_{xx}+\epsilon_{yy}+\epsilon_{zz})$.
[b] $\Delta\epsilon_\infty = \epsilon_{zz} - \frac{1}{2}(\epsilon_{xx}+\epsilon_{yy})$.
[c] UR: uncoupled response.
[d] FP: full potential; PP: pseudopotential; ASA: atomic-sphere approximation.
[e] PW: plane wave; LMTO: linearized muffin-tin orbitals; LCAO: linear combination of atomic orbitals.
[f] LF: local-field effects.

$\sqrt{8/3}$ and the internal parameter $u = 3/8$. In Table III we summarize the geometrical parameters, the calculated isotropic average values for the dielectric constant $\bar{\epsilon}_\infty$ and the anisotropy $\Delta\epsilon_\infty$ in this dielectric constant, together with the experimental values for $\bar{\epsilon}_\infty$,[51–55] and relative errors compared to these experimental values. We have also included other theoretical results (UR) for $\bar{\epsilon}_\infty$ and $\Delta\epsilon_\infty$ found by Xu *et al.*[18] (FP), Chen *et al.*[19] (PP), Christensen *et al.*[20] (LMTO-ASA), and Wang *et al.*[21] (PP). The isotropic average values for the dielectric constant is defined as $\bar{\epsilon}_\infty = \frac{1}{3}(\epsilon_{xx}+\epsilon_{yy}+\epsilon_{zz})$ and the anisotropy as $\Delta\epsilon_\infty = \epsilon_{zz} - \frac{1}{2}(\epsilon_{xx}+\epsilon_{yy})$. Our results for $\bar{\epsilon}_\infty$ showed substantial differences from the theoretical results found by others,[18–21] and an average deviation of about 5% from the experimental values,[51–55] which is a substantial improvement over the other theoretical methods.

### D. Diamond structure

The calculations for the diamond structures were performed by using 175 symmetry unique **k** points in the IBZ for the (numerical) integrations in the reciprocal space, and using the standard $3Z2P$ NAO/STO basis. In Table IV we list for carbon (C), silicon (Si), and germanium (Ge) the lattice constants, the calculated dielectric constants $\epsilon_\infty$ of this work together with the experimental values,[36–39,49] and relative errors compared to these experimental values. Other theoretical results of Refs. 7, 12, 13, and 22–30 are also included. Our results for $\epsilon_\infty$ show an average deviation of about 5% from the experimental values,[36] and compared to other theoretical investigations, it can be seen from Table IV that our results are again of better quality.

### E. Zinc-blende structure

The zinc-blende structures we studied can be grouped into the III-V (AlP, AlAs, AlSb, GaP, GaAs, GaSb, InP, InAs, InSb) and the II-VI (ZnS, ZnSe, ZnTe, CdS, CdSe, CdTe) compounds. These calculations were done using the same $3Z2P$ NAO/STO basis and **k** space integration accuracy as for the diamond structures.

#### *1. III-V compounds*

The calculated dielectric constants for these compounds are collected in Table V, together with the lattice constants, the experimental values for $\epsilon_\infty$,[39–42,50] the errors compared to these experimental values, and other theoretical results.[22,25–31] We find that our results for $\epsilon_\infty$ are closer to experiment than those found by others,[22,29,30] with the exception of InSb, for which we find an underestimation of about 40%. At the same time we find a considerable overestimation of the experimental band gap for this small-gap semiconductor, as can be seen in Table VII. In this calculation we have included the $4d$ atomic states in the valence basis, as these give rise to shallow core states, which can affect the position of the valence-band maximum.[33,34] The overestimation of the band gap is in clear contrast with the general trend observed in LDA-DFT band-structure calculations, i.e., that the band

TABLE IV. Optical dielectric constants for crystals in the diamond lattice structure.

| Solid | $a$ (Å) (Ref. 36) | This work | Experiment | Error (%) | Other theory | Method [a b c d] |
|---|---|---|---|---|---|---|
| C | 3.57 | 5.62 | 5.7 (Ref. 36) | 1 | 5.90 (Ref. 7) | DM,PP,PW,LF,XC |
| | | | 5.7 (Ref. 37) | 1 | 4.34 (Ref. 22) | UR,FP,LCAO |
| | | | 5.67 (Ref. 49) | 1 | 5.20–5.86 (Ref. 24) | DM,PP,PW,LF,QP |
| | | | | | 5.5 (Ref. 27) | DM,PP,LCGO,LF,QP |
| | | | | | 5.7 (Ref. 29) | UR,EP,LCAO |
| Si | 5.43 | 12.78 | 12.0 (Ref. 36) | 7 | 12.9 (Ref. 7) | DM,PP,PW,LF,XC |
| | | | 11.4 (Ref. 38) | 12 | 9.03 (Ref. 22) | UR,FP,LCAO |
| | | | | | 12.7 (Ref. 12) | DM,PP,PW,LF,XC |
| | | | | | 11.2 (Ref. 13) | DM,PP,PW,LF,QP |
| | | | | | 12.4–12.9(Ref. 23) | DFPT,PP,PW,LF,XC |
| | | | | | 12.7 (Ref. 25) | DFPT,PP,PW,LF,XC |
| | | | | | 12.05 (Ref. 26) | DM,FP,LMTO,LF,QP |
| | | | | | 12.8 (Ref. 27) | DM,PP,LCGO,LF,QP |
| | | | | | 11.7 (Ref. 28) | UR,PP,LCGO,QP |
| | | | | | 12.0 (Ref. 29) | UR,EP,LCAO |
| | | | | | 13.6 (Ref. 30) | DFPT,PP,PW,LF,XC |
| Ge | 5.66 | 16.22 | 16.0 (Ref. 36) | 1 | 20.7 (Ref. 7) | DM,PP,PW,LF,XC |
| | | | 15.3 (Ref. 38) | 6 | 12.31 (Ref. 22) | UR,FP,LCAO |
| | | | 15.3 (Ref. 39) | 6 | 16.5 (Ref. 13) | DM,PP,PW,LF,QP |
| | | | | | 15.58 (Ref. 26) | DM,FP,LMTO,LF,QP |
| | | | | | 21.8 (Ref. 27) | DM,PP,LCGO,LF,QP |
| | | | | | 16.0 (Ref. 28) | UR,PP,LCGO,QP |
| | | | | | 16.0 (Ref. 29) | UR,EP,LCAO |
| | | | | | 18.7 (Ref. 30) | DFPT,PP,PW,LF,XC |

[a]DFPT: density-function perturbation theory; DM: dielectric matrix; UR: uncoupled response.

[b]FP: full potential; PP: pseudopotential; EP: empirical potential.

[c]PW: plane wave; LMTO: linearized muffin-tin orbitals; LCAO: linear combination of atomic orbitals; LCGO: linear combination of Gaussian orbitals.

[d]XC: exchange-correlation effects; QP: quasiparticle energy shift; LF: local-field effects.

gap tends to be underestimated in semiconductors. However, inclusion of scalar relativistic corrections stabilizes the *s*-like conduction-band minimum considerably. In the LDA this causes the gap even to vanish, thus incorrectly predicting the InSb crystal to be a semimetal, as was found in full-potential scalar relativistic LAPW calculations,[34] and as we have checked in our ground-state calculations. We are not yet able to include these scalar relativistic corrections in the time-dependent calculations. Nevertheless, with the exception of the InSb crystal, we find an average deviation of about 4% from experiment for the III-V compounds.

#### *2. II-VI compounds*

Our results for the calculated dielectric constants $\epsilon_\infty$ are collected in Table VI, together with experimental values[42–46] and other theoretical investigations.[22,28] We find that our results for $\epsilon_\infty$ show an average deviation of about 9% from experiment, and are comparable to those found by Huang *et al.*[22] (UR, FP) and Wang *et al.*[28] (UR, PP), except for the Te compounds, where our results are substantially better.

## IV. DIELECTRIC FUNCTIONS

The dielectric functions $\epsilon(\omega)$ for all zinc-blende structures (which reduces to the diamond structure in case of group IV elementary solids) were calculated using the same $3Z2P$ NAO/STO basis and **k** space integration accuracy as mentioned before for calculating the dielectric constants of the diamond and zinc-blende structures. We report the dielectric functions $\epsilon(\omega)$ for a selected range of compounds, for which experimental data was available. The calculated dielectric functions for the remaining compounds are available on request. When comparing our calculated dielectric functions with the experiment ones, we found all features uniformly shifted to lower energies. Therefore, in order to facilitate the comparison with experiment, we shifted the calculated results for the dielectric functions to higher energies, in such a way that the zero crossings in the calculated $\mathrm{Re}[\epsilon(\omega)]$ coincided with the experimental zero crossings. The values for the applied shifts to the calculated dielectric functions are compared in Table VII with the LDA and the experimental band gap ($E_g$).[67] As can be seen from Table VII, there is no direct relation between the applied shifts and the error in the LDA band gap for these compounds. The calculated (shifted) dielectric functions $\epsilon(\omega)$ for C, Si, and Ge are depicted in Figs. 1, 2, and 3, together with the experimental data of Palik[56] and Aspnes *et al.*[57] These spectra are in very good agreement with the experimental spectra, there are, however, features that need improvement. The $E_2$ peak[68] for C, Si, and Ge (high-energy peak in $\mathrm{Im}[\epsilon(\omega)]$) is too

TABLE V. Optical dielectric constants for crystals in the III-V zinc-blende lattice structure.

| Solid | $a$ (Å) (Ref. 36) | This work | Experiment | Error (%) | Other theory | Method [a b c d] |
|---|---|---|---|---|---|---|
| AlP | 5.45 | 8.16 | 8.0 (Ref. 39) | 2 | 5.63 (Ref. 22) | UR,FP,LCAO |
| AlAs | 5.62 | 8.83 | 8.16 (Ref. 40) | 8 | 6.81 (Ref. 22) | UR,FP,LCAO |
| | | | | | 9.2 (Ref. 30) | DFPT,PP,PW,LF,XC |
| AlSb | 6.13 | 10.22 | 10.2 (Ref. 41) | 1 | 7.21 (Ref. 22) | UR,FP,LCAO |
| | | | | | 12.2 (Ref. 30) | DFPT,PP,PW,LF,XC |
| GaP | 5.45 | 9.59 | 9.1 (Ref. 42) | 5 | 9.29 (Ref. 22) | UR,FP,LCAO |
| | | | | | 9.4 (Ref. 28) | UR,PP,LCGO,QP |
| | | | | | 9.1 (Ref. 29) | UR,EP,LCAO |
| GaAs | 5.65 | 11.33 | 10.9 (Ref. 41) | 4 | 11.21 (Ref. 22) | UR,FP,LCAO |
| | | | 10.8 (Ref. 50) | 5 | 12.3 (Ref. 25) | DFPT,PP,PW,LF,XC |
| | | | | | 10.83 (Ref. 26) | DM,FP,LMTO,LF,QP |
| | | | | | 13.1 (Ref. 27) | DM,PP,LCGO,LF,QP |
| | | | | | 10.9 (Ref. 28) | UR,PP,LCGO,QP |
| | | | | | 10.9 (Ref. 29) | UR,EP,LCAO |
| | | | | | 12.3 (Ref. 30) | DFPT,PP,PW,LF,XC |
| | | | | | 10.2 (Ref. 31) | DM,PP,PW,LF,QP |
| GaSb | 6.12 | 13.54 | 14.4 (Ref. 41) | 6 | 11.42(Ref. 22) | UR,FP,LCAO |
| | | | | | 14.4 (Ref. 29) | UR,EP,LCAO |
| | | | | | 18.1 (Ref. 30) | DFPT,PP,PW,LF,XC |
| InP | 5.87 | 9.60 | 9.6 (Ref. 41) | 0 | 7.92 (Ref. 22) | UR,FP,LCAO |
| | | | | | 9.6 (Ref. 29) | UR,EP,LCAO |
| InAs | 6.04 | 11.40 | 12.3 (Ref. 41) | 7 | 10.02(Ref. 22) | UR,FP,LCAO |
| | | | | | 12.3 (Ref. 29) | UR,EP,LCAO |
| InSb | 6.48 | 9.15 | 15.7 (Ref. 41) | 42 | 13.51(Ref. 22) | UR,FP,LCAO |
| | | | | | 15.7 (Ref. 29) | UR,EP,LCAO |

[a]DFPT: density-function perturbation theory; DM: dielectric matrix; UR: uncoupled response.
[b]FP: full potential; PP: pseudopotential; EP: empirical potential.
[c]PW: plane wave; LMTO: linearized muffin-tin orbitals; LCAO: linear combination of atomic orbitals; LCGO: linear combination of Gaussian orbitals.
[d]XC: exchange-correlation effects; QP: quasiparticle energy shift, LF: local-field effects.

sharp, and its magnitude is overestimated compared to experiment. Looking at the $E_1$ peak in Si and Ge (low-energy peak in $\mathrm{Im}[\epsilon(\omega)]$), we see that it is underestimated in amplitude and appears as a shoulder, which can be ascribed to a failure in the description of excitonic effects (screened Coulomb attraction between electron and hole). The sharp structures which were found in the calculated spectra at energies higher than the $E_2$ peak, were much less pronounced in experiment.

The calculated (shifted) dielectric functions $\epsilon(\omega)$ for the

TABLE VI. Optical dielectric constants for crystals in the II-VI zinc-blende lattice structure.

| Solid | $a$ (Å) (Ref. 36) | This work | Experiment | Error (%) | Other theory | Method [a b c d] |
|---|---|---|---|---|---|---|
| ZnS | 5.41 | 5.71 | 5.2 (Ref. 43) | 10 | 5.63 (Ref. 22) | UR,FP,LCAO |
| | | | | | 5.5 (Ref. 28) | UR,PP,LCGO,QP |
| ZnSe | 5.67 | 6.74 | 5.9 (Ref. 44) | 14 | 5.56 (Ref. 22) | UR,FP,LCAO |
| | | | | | 6.6 (Ref. 28) | UR,PP,LCGO,QP |
| ZnTe | 6.09 | 7.99 | 7.3 (Ref. 45) | 9 | 5.24 (Ref. 22) | UR,FP,LCAO |
| CdS | 5.82 | 4.89 | 5.2 (Ref. 46) | 6 | 5.05 (Ref. 22) | UR,FP,LCAO |
| CdSe | 6.08 | 6.26 | 5.8 (Ref. 44) | 8 | 5.68 (Ref. 22) | UR,FP,LCAO |
| CdTe | 6.48 | 6.70 | 7.2 (Ref. 45) | 7 | 9.02 (Ref. 22) | UR,FP,LCAO |

[a]UR: uncoupled response.
[b]FP: full potential; PP: pseudopotential.
[c]LCAO: linear combination of atomic orbitals; LCGO: linear combination of Gaussian orbitals.
[d]QP: quasiparticle energy shift.

TABLE VII. The calculated LDA band gaps and the experimental values, in comparison with the applied energy shifts to the dielectric functions for the crystals in Figs. 1–13. All values are given in electron volts (eV).

| Solid | $E_g$ (Experiment) (Ref. 67) | $E_g$ (LDA) | $\Delta$ [a] | Applied shift |
|---|---|---|---|---|
| C | 5.47 | 4.14 | 1.33 | 0.60 |
| Si | 1.11 | 0.55 | 0.56 | 0.40 |
| Ge | 0.67 | 0.39 | 0.28 | 0.30 |
| GaP | 2.24 | 1.50 | 0.74 | 0.50 |
| GaAs | 1.35 | 1.02 | 0.33 | 0.45 |
| GaSb | 0.67 | 0.79 | −0.12 | 0.30 |
| InP | 1.27 | 1.00 | 0.27 | 0.40 |
| InAs | 0.36 | 0.47 | −0.11 | 0.35 |
| InSb | 0.17 | 0.99 | −0.82 | 0.15 |
| ZnS | 3.54 | 2.06 | 1.48 | 0.90 |
| ZnSe | 2.58 | 1.52 | 1.06 | 1.05 |
| ZnTe | 2.26 | 1.99 | 0.27 | 0.70 |
| CdTe | 1.44 | 1.70 | −0.26 | 0.65 |

[a] $\Delta = E_g$ (experiment) $- E_g$ (LDA).

Ga and In series are depicted in Figs. 4–9, together with the experimental data of Aspnes *et al.*[57] The $\epsilon(\omega)$ for the Zn series and CdTe are depicted in Figs. 10–13, together with the experimental data of Freelouf.[58] The experimental data of Freelouf[58] for the imaginary parts of the dielectric functions $\epsilon(\omega)$ have been obtained by digitizing the data in their plots. The real parts have been obtained as the Kramers-Kronig transform of these imaginary parts. The result of applying a

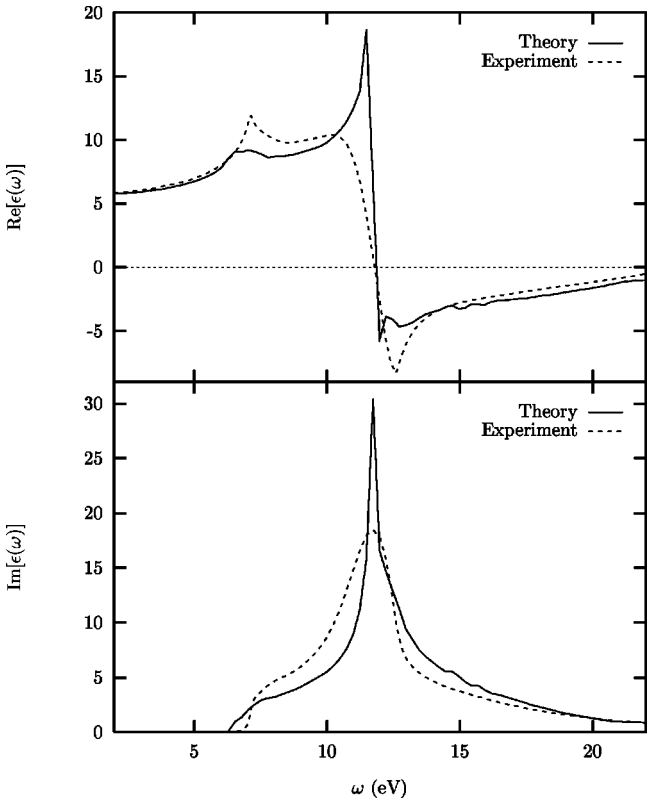


FIG. 1. Plots of the real and imaginary part of the calculated dielectric function of diamond (C) in comparison with the experimental data (Ref. 57).

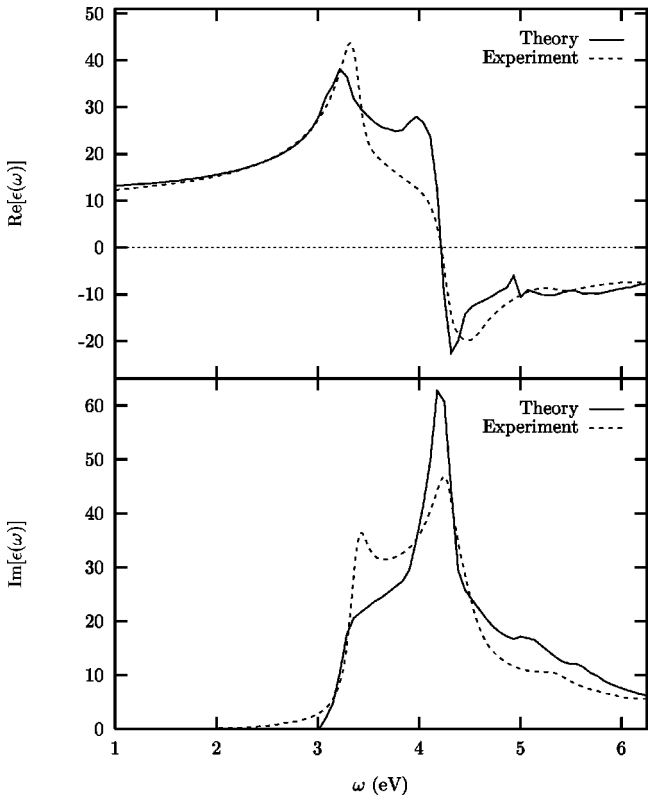


FIG. 2. Plots of the real and imaginary part of the calculated dielectric function of silicon (Si) in comparison with the experimental data (Refs. 56 and 57).

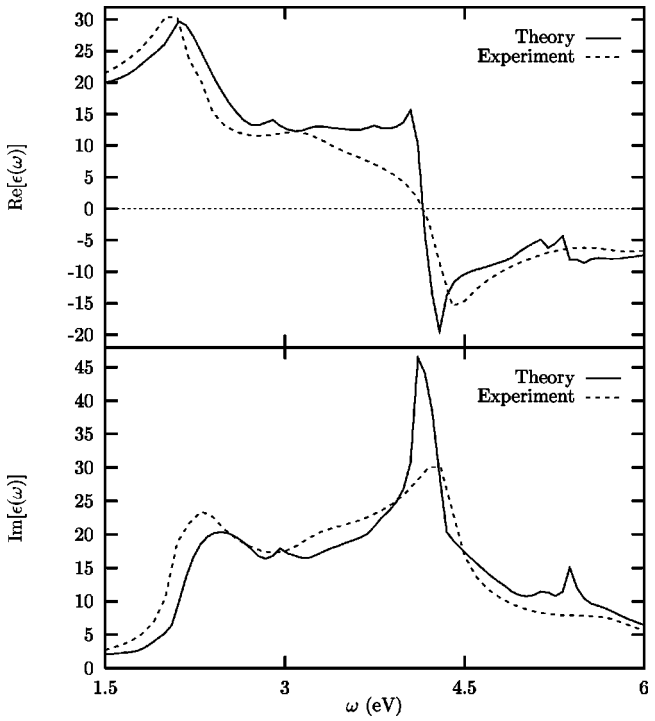


FIG. 3. Plots of the real and imaginary part of the calculated dielectric function of germanium (Ge) in comparison with the experimental data (Ref. 57).

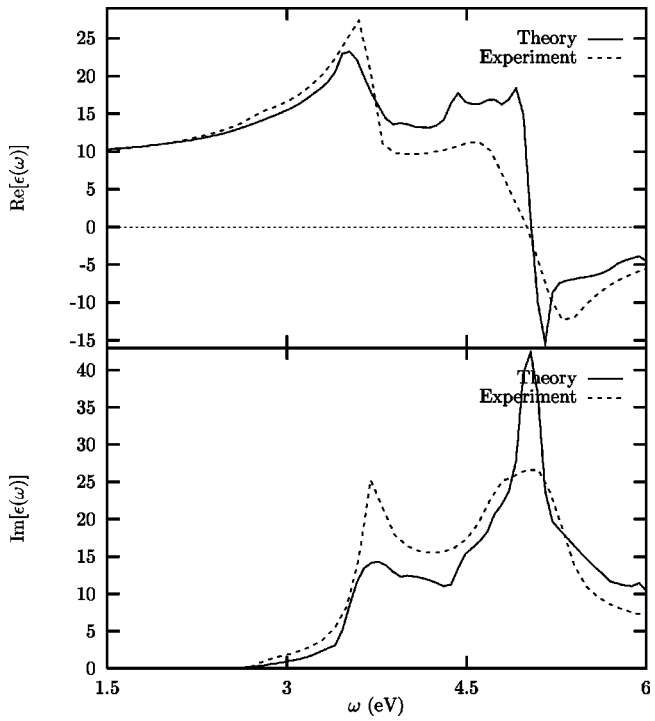


FIG. 4. Plots of the real and imaginary part of the calculated dielectric function of gallium phosphide (GaP) in comparison with the experimental data (Ref. 57).

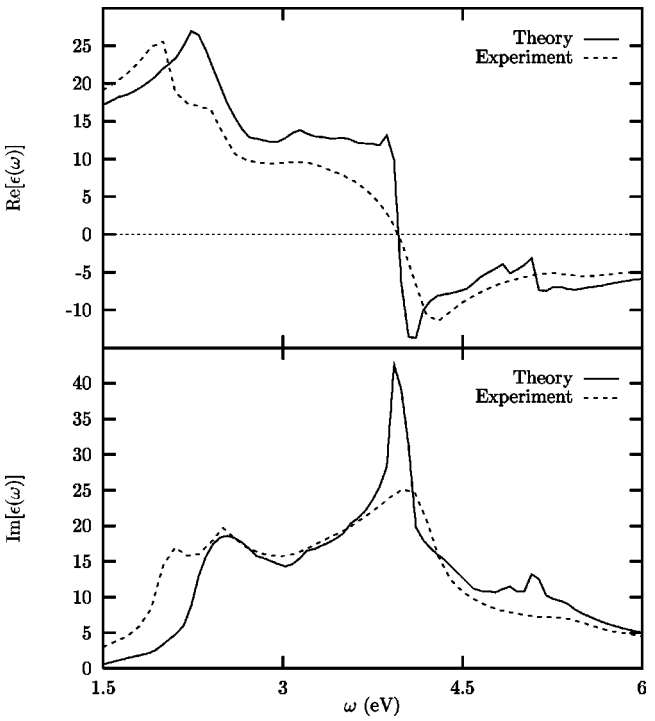


FIG. 6. Plots of the real and imaginary part of the calculated dielectric function of gallium antimonide (GaSb) in comparison with the experimental data (Ref. 57).

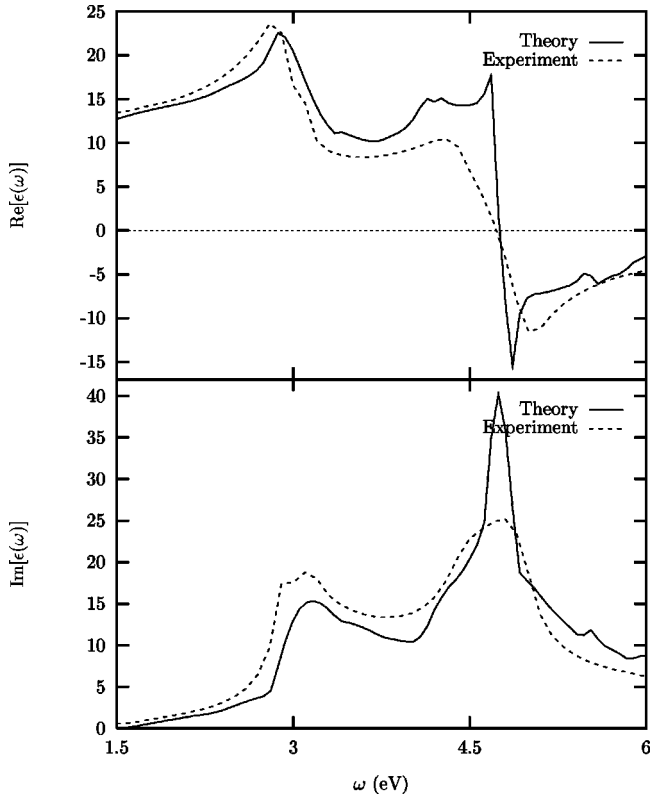


FIG. 5. Plots of the real and imaginary part of the calculated dielectric function of gallium arsenide (GaAs) in comparison with the experimental data (Ref. 57).

shift to our calculated dielectric functions for these compounds is that we find an overall agreement between our spectra and the experimental spectra which is quite good. However, when looking in more detail, we find that the $E_2$ peaks coincide with experiment, but are (also in these com-

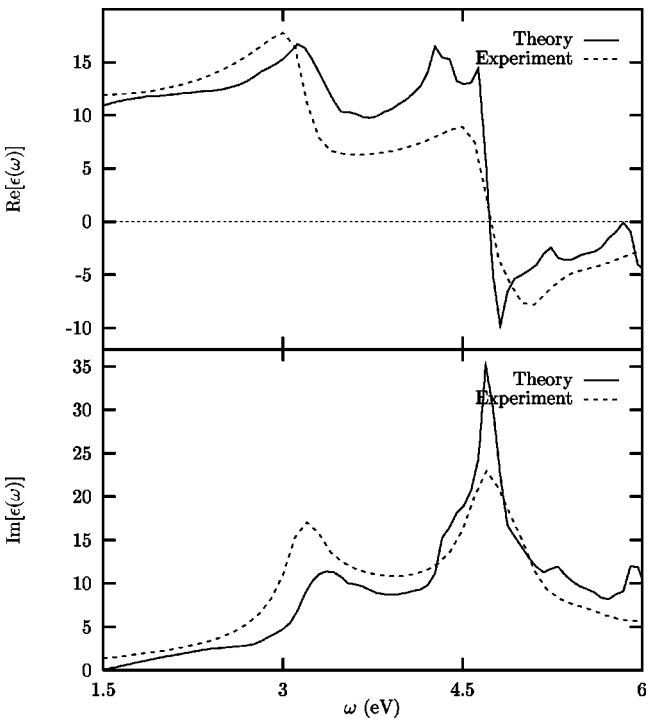


FIG. 7. Plots of the real and imaginary part of the calculated dielectric function of indium phosphide (InP) in comparison with the experimental data (Ref. 57).

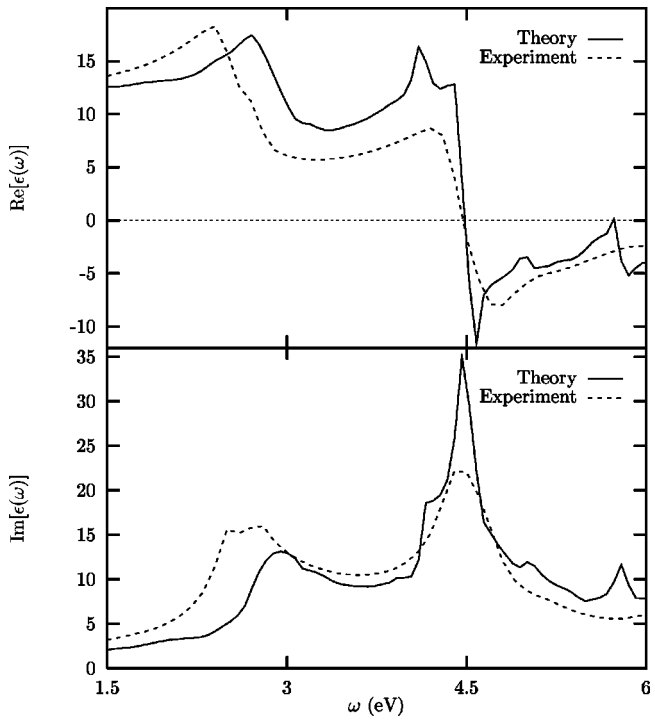


FIG. 8. Plots of the real and imaginary part of the calculated dielectric function of indium arsenide (InAs) in comparison with the experimental data (Ref. 57).

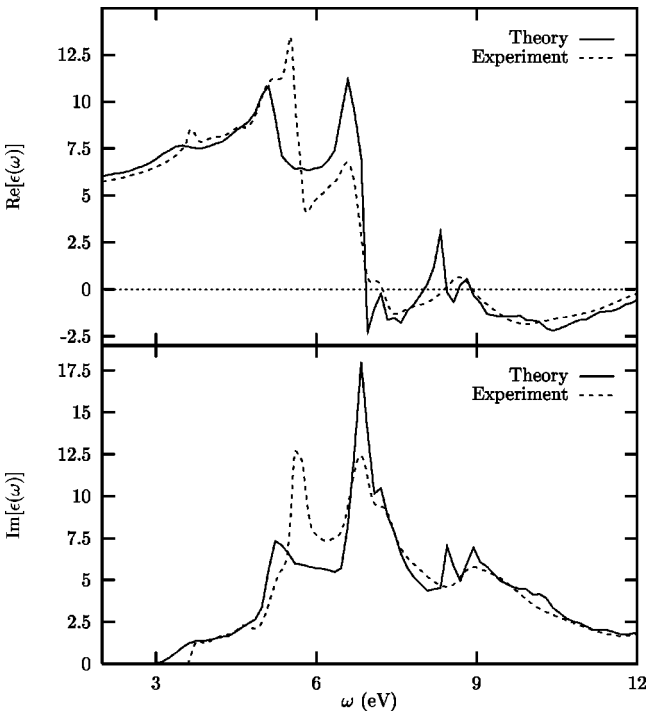


FIG. 10. Plots of the real and imaginary part of the calculated dielectric function of zinc sulfide (ZnS) in comparison with the experimental data (Ref. 58).

pounds) too sharp and their magnitudes are still overestimated compared to experiment. Looking at the $E_1$ peaks, we see that they are underestimated in amplitude and in general too close to the $E_2$ peak. Further, the calculated $E_1$ peaks do not reproduce the experimental double peak structure for the As, Sb, Se, and Te compounds. The sharp structures in the calculated dielectric functions at energies higher than the $E_2$ peak are less pronounced in experiment.

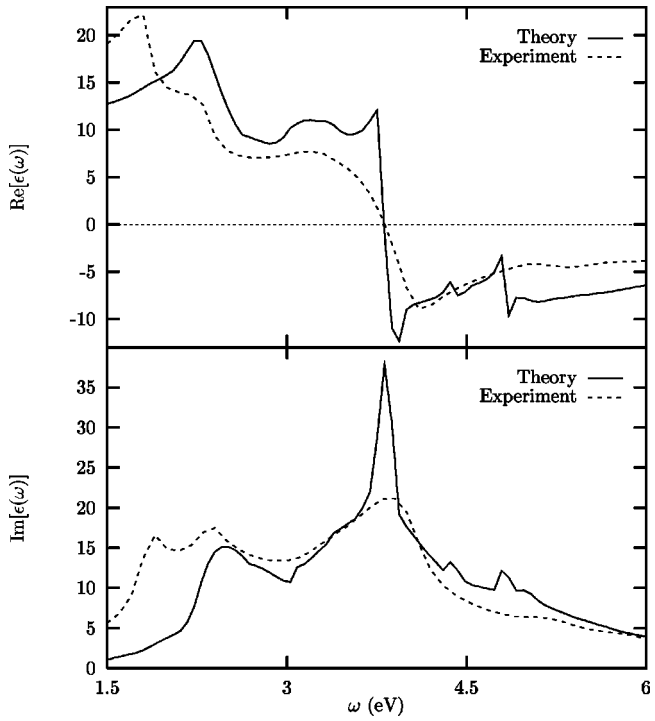


FIG. 9. Plots of the real and imaginary part of the calculated dielectric function of indium antimonide (InSb) in comparison with the experimental data (Ref. 57).

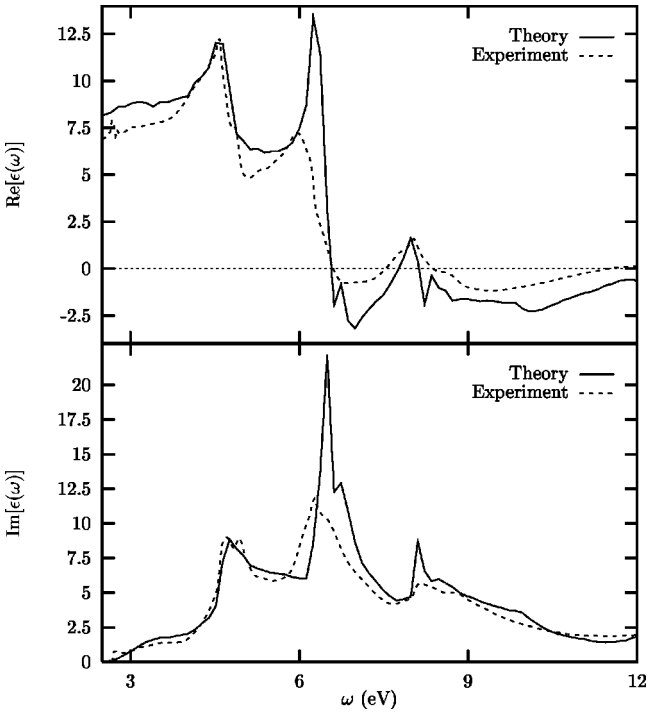


FIG. 11. Plots of the real and imaginary part of the calculated dielectric function of zinc selenide (ZnSe) in comparison with the experimental data (Ref. 58).

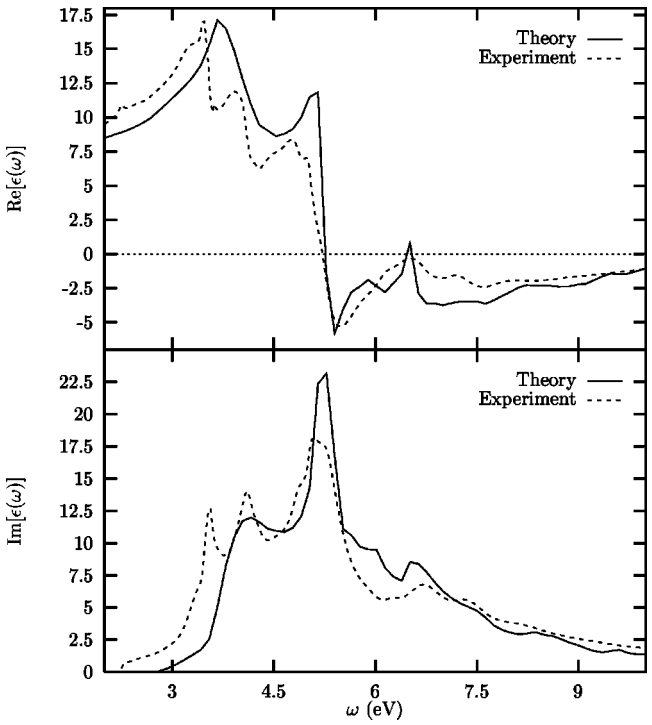


FIG. 12. Plots of the real and imaginary part of the calculated dielectric function of zinc telluride (ZnTe) in comparison with the experimental data (Ref. 58).

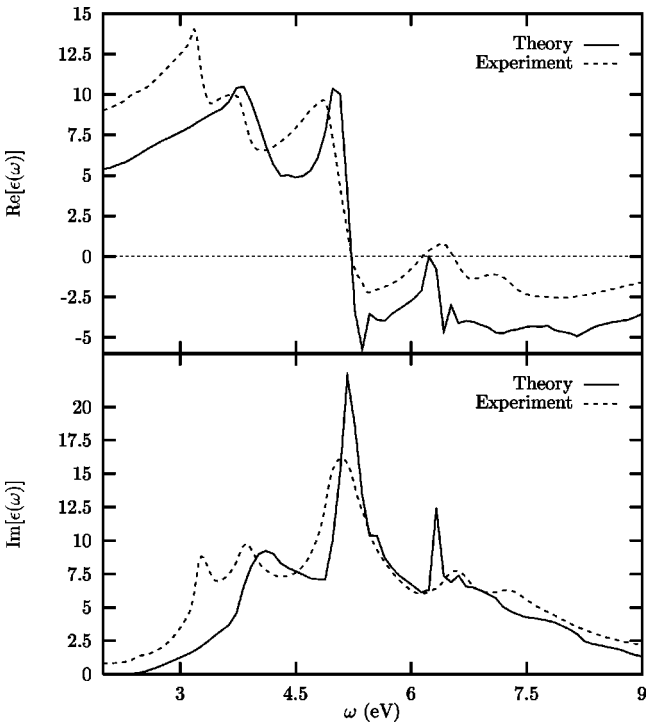


FIG. 13. Plots of the real and imaginary part of the calculated dielectric function of cadmium telluride (CdTe) in comparison with the experimental data (Ref. 58).

## V. CONCLUSIONS

The dielectric function of a large range of nonmetallic crystals, of various lattice types, is calculated by using an efficient, accurate, and rapidly converging real-space implementation of time-dependent density-functional theory. In this method we employ a lattice periodic (microscopic) effective scalar potential in combination with a uniform (macroscopic) electric field. Our results for the dielectric constants $\epsilon_\infty$ (at optical frequencies) were obtained without the use of a scissors operator. They are in good agreement with experiment and in general more accurate than those found by others. The accuracy of our calculated $\epsilon_\infty$ values for crystals is comparable with the TDDFT results for polarizabilities in molecular systems. On average we find a deviation of 4–5 % from experiment for the group IV and III-V compounds in the wurtzite, zinc-blende, and diamond lattice structure, 8–9 % for the II-VI and I-VII compounds in the zinc-blende and sodium chloride lattice structure, and up to 14% deviation for the fluoride lattice structure. Therefore we observe a trend that the accuracy of the results is reduced in the strongly ionic compounds. The calculated dielectric functions $\epsilon(\omega)$ reproduce the experimental spectral features quite accurately, although there is a more or less uniform shift necessary between the experimental and theoretical spectra.

[1] P. Hohenberg and W. Kohn, Phys. Rev. **136**, B864 (1964).
[2] W. Kohn and L. J. Sham, Phys. Rev. **140**, A1133 (1965).
[3] S. J. A. van Gisbergen, J. G. Snijders, and E. J. Baerends, J. Chem. Phys. **103**, 9347 (1995).
[4] S. J. A. van Gisbergen, V. P. Osinga, O. V. Gritsenko, R. van Leeuwen, J. G. Snijders, and E. J. Baerends, J. Chem. Phys. **105**, 3142 (1996).
[5] S. J. A. van Gisbergen, F. Kootstra, P. R. T. Schipper, O. V. Gritsenko, J. G. Snijders, and E. J. Baerends, Phys. Rev. A **57**, 2556 (1998).
[6] O. Gunnarsson and R. O. Jones, Phys. Scr. **21**, 394 (1980).
[7] M. S. Hybertsen and S. G. Louie, Phys. Rev. B **35**, 5585 (1987).
[8] Z. H. Levine and S. G. Louie, Phys. Rev. B **25**, 6310 (1982).
[9] Y. T. Shen, D. M. Bylander, and L. Kleinman, Phys. Rev. B **36**, 3465 (1987).
[10] E. Runge and E. K. U. Gross, Phys. Rev. Lett. **52**, 997 (1984).
[11] S. J. A. van Gisbergen, J. G. Snijders, and E. J. Baerends, Comput. Phys. Commun. **118**, 119 (1999).
[12] S. Baroni and R. Resta, Phys. Rev. B **33**, 7017 (1986).
[13] Z. H. Levine and D. C. Allan, Phys. Rev. B **43**, 4187 (1991); **44**, 12 781 (1991); Phys. Rev. Lett. **63**, 1719 (1989); **66**, 41 (1991).
[14] M. S. Hybertsen and S. G. Louie, Phys. Rev. B **34**, 5390 (1986).
[15] F. Kootstra, P. L. de Boeij, and J. G. Snijders, J. Chem. Phys. **112**, 6517 (2000).
[16] W. Y. Ching, F. Gan, and M. Z. Huang, Phys. Rev. B **52**, 1596 (1995).
[17] J. Li, C. Duan, Z. Gu, and D. Wang, Phys. Rev. B **57**, 2222 (1998).
[18] Y. N. Xu and W. Y. Ching, Phys. Rev. B **48**, 4335 (1993).
[19] J. Chen, Z. H. Levine, and J. W. Wilkins, Appl. Phys. Lett. **66**, 1129 (1995).
[20] N. E. Christensen and I. Gorczyca, Phys. Rev. B **50**, 4397 (1994).

[21] R. Wang, P. P. Ruden, J. Kolnik, I. Oguzman, and K. F. Brennan, J. Phys. Chem. Solids **58**, 913 (1997).
[22] M. Z. Huang and W. Y. Ching, Phys. Rev. B **47**, 9449 (1993).
[23] A. Dal Corso, S. Baroni, and R. Resta, Phys. Rev. B **49**, 5323 (1994).
[24] J. Chen, Z. H. Levine, and J. W. Wilkins, Phys. Rev. B **50**, 11 514 (1994).
[25] S. Baroni, P. Giannozzi, and A. Testa, Phys. Rev. Lett. **58**, 1861 (1987).
[26] M. Alouani and J. Wills, Phys. Rev. B **54**, 2480 (1996).
[27] M. Rohlfing, P. Krüger, and J. Pollmann, Phys. Rev. B **48**, 17 791 (1993).
[28] C. S. Wang and B. M. Klein, Phys. Rev. B **24**, 3417 (1981).
[29] D. J. Moss, E. Ghahramani, J. E. Sipe, and H. M. van Driel, Phys. Rev. B **34**, 8758 (1986).
[30] P. Giannozzi, S. de Gironcoli, P. Pavone, and S. Baroni, Phys. Rev. B **43**, 7231 (1991).
[31] O. Pulci, G. Onida, A. I. Shkrebtii, R. Del Sole, and B. Adolph, Phys. Rev. B **55**, 6685 (1997).
[32] F. Gan, Y. Xu, M. Huang, W. Y. Ching, and J. G. Harrison, Phys. Rev. B **45**, 8248 (1992).
[33] M. Cardona, N. E. Christensen, and G. Fasol, Phys. Rev. B **38**, 1806 (1988).
[34] G. Y. Guo, J. Crain, P. Blaha, and W. M. Temmerman, Phys. Rev. B **47**, 4841 (1993).
[35] M. E. Lines, Phys. Rev. B **41**, 3372 (1990).
[36] N. W. Ashcroft and N. D. Mermin, *Solid State Physics* (Holt, Rinehart, and Winston, New York, 1976).
[37] N. A. Goryuneva, in *Chemistry of Diamond-like Semiconductors* (Chapman and Hall, London, 1965), p. 115.
[38] H. H. Li, J. Chem. Phys. Ref. Data **9**, 561 (1980).
[39] As listed in W. A. Harrison, *Electronic Structure and the Properties of Solids* (Freeman, San Francisco, 1980).
[40] R. E. Fern and A. Onton, J. Appl. Phys. **42**, 3499 (1971).
[41] E. Burstein, H. Brodsky, and G. Lucousky, Int. J. Quantum Chem. **1**, 756 (1967).
[42] A. S. Barker, Jr., Phys. Rev. **165**, 917 (1968).
[43] S. J. Czyzak, W. M. Barker, R. C. Crane, and J. B. Howe, J. Opt. Soc. Am. **47**, 240 (1957).
[44] A. Manabe, A. Mitsuishi, and H. Yoshinaga, Jpn. J. Appl. Phys. **6**, 593 (1967).
[45] D. T. F. Marple, J. Appl. Phys. **35**, 539 (1964).
[46] T. M. Bieniewski and S. J. Czyzak, J. Opt. Soc. Am. **53**, 496 (1963).
[47] J. Barth, R. L. Johnson, and M. Cardona, Phys. Rev. B **41**, 3291 (1990).
[48] G. Stephan, Y. le Calvez, J. C. Lemonier, and S. Robin, J. Phys. Chem. Solids **30**, 601 (1969).
[49] *Numerical Data and Functional Relationships in Science and Technology*, edited by O. Madelung, Landolt-Börnstein, New Series, Group III, Vol. 17, Pt. A (Springer Verlag, New York, 1982).
[50] K. B. Kahen and J. P. Leburton, Phys. Rev. B **32**, 5177 (1985).
[51] A. T. Collins, E. C. Lightowlers, and P. J. Dean, Phys. Rev. **158**, 833 (1967).
[52] L. Akasaki and M. Hashimoto, Solid State Commun. **5**, 851 (1967).
[53] E. Ejder, Phys. Status Solidi A **5**, 445 (1971).
[54] P. Perlin, I. Gorczyca, N. E. Christensen, I. Grzegory, H. Teisseyre, and T. Suski, Phys. Rev. B **45**, 13 307 (1992); P. Perlin, I. Gorczyca, S. Porowski, T. Suski, N. E. Christensen, and A. Polian, Jpn. J. Appl. Phys., Part 1 **32**, 334 (1993).
[55] J. Misek and F. Srobar, Elektrotech. Cas. **30**, 690 (1979).
[56] *Handbook of Optical Constants of Solids*, edited by E. D. Palik (Academic, New York, 1985).
[57] P. E. Aspnes and A. A. Studna, Phys. Rev. B **27**, 985 (1983).
[58] J. L. Freelouf, Phys. Rev. B **7**, 3810 (1973).
[59] G. te Velde and E. J. Baerends, Phys. Rev. B **44**, 7888 (1991); J. Comput. Phys. **99**, 84 (1992).
[60] C. Fonseca Guerra, O. Visser, J. G. Snijders, G. te Velde, and E. J. Baerends, in *Methods and Techniques in Computational Chemistry*, edited by E. Clementi and G. Corongiu (STEF, Gagliary, 1995), p. 305.
[61] S. H. Vosko, L. Wilk, and M. Nusair, Can. J. Phys. **58**, 1200 (1980).
[62] F. Herman and S. Skillman, *Atomic Structure Calculations* (Prentice-Hall, Englewood Cliffs, NJ, 1963).
[63] G. te Velde, Ph.D. thesis, Free University, Amsterdam, 1990.
[64] E. J. Baerends, D. E. Ellis, and P. Ros, Chem. Phys. **2**, 41 (1973).
[65] G. Wiesenekker, G. te Velde, and E. J. Baerends, J. Phys. C **21**, 4263 (1988).
[66] G. Wiesenekker and E. J. Baerends, J. Phys.: Condens. Matter **3**, 6721 (1991).
[67] *CRC Handbook of Chemistry and Physics*, 80th Edition (CRC Press, Boca Raton, 1999).
[68] Cf. nomenclature, e.g., M. Cardona, *Modulation Spectroscopy* (Academic Press, New York, 1969).